



CHORUS

This is the accepted manuscript made available via CHORUS. The article has been published as:

Engineering Carrier Effective Masses in Ultrathin Quantum Wells of IrO₂

Jason K. Kawasaki, Choong H. Kim, Jocienne N. Nelson, Sophie Crisp, Christian J. Zollner, Eric Biegenwald, John T. Heron, Craig J. Fennie, Darrell G. Schlom, and Kyle M. Shen

Phys. Rev. Lett. **121**, 176802 — Published 25 October 2018

DOI: [10.1103/PhysRevLett.121.176802](https://doi.org/10.1103/PhysRevLett.121.176802)

Engineering Carrier Effective Masses in Ultrathin Quantum Wells of IrO₂

Jason K. Kawasaki,^{1,2,3,4,*} Choong H. Kim,^{5,6} Jocienne N. Nelson,² Sophie Crisp,² Christian J. Zollner,⁷
Eric Biegenwald,³ John T. Heron,³ Craig J. Fennie,⁷ Darrell G. Schlom,^{1,3} and Kyle M. Shen^{1,2,†}

¹*Kavli Institute at Cornell for Nanoscale Science, Cornell University, Ithaca NY 14853*

²*Laboratory for Atomic and Solid State Physics, Cornell University, Ithaca NY 14853*

³*Department of Materials Science and Engineering, Cornell University, Ithaca NY 14853*

⁴*Department of Materials Science and Engineering, University of Wisconsin, Madison WI 53706*

⁵*Center for Correlated Electron Systems, Institute for Basic Science, Seoul, Korea*

⁶*Department of Physics and Astronomy, Seoul National University, Seoul, Korea*

⁷*Department of Applied and Engineering Physics, Cornell University, Ithaca NY 14853*

(Dated: October 3, 2018)

The carrier effective mass plays a crucial role in modern electronic, optical, and catalytic devices, and is fundamentally related to key properties of solids such as the mobility and density of states. Here we demonstrate a method to deterministically engineer the effective mass using spatial confinement in metallic quantum wells of the transition metal oxide IrO₂. Using a combination of *in situ* angle-resolved photoemission spectroscopy measurements in conjunction with precise synthesis by oxide molecular-beam epitaxy, we show that the low-energy electronic sub-bands in ultrathin films of rutile IrO₂ have their effective masses enhanced by up to a factor of six with respect to the bulk. The origin of this strikingly large mass enhancement is the confinement-induced quantization of the highly non-parabolic, three-dimensional electronic structure of IrO₂ in the ultrathin limit. This mechanism lies in contrast to that observed in other transition metal oxides, in which mass enhancement tends to result from complex electron-electron interactions and is difficult to control. Our results demonstrate a general route towards the deterministic enhancement and engineering of carrier effective masses in spatially confined systems, based on an understanding of the three-dimensional bulk electronic structure.

Quantum confinement is an essential ingredient for exploring the fundamental physics of two-dimensional electron systems, and for modern technologies as devices become scaled down to the atomically thin limit. In the simplest picture, confinement in the out-of-plane direction results in quantized, two-dimensional sub-bands. In nearly all so-called “quantum well” systems investigated to date (e.g., semiconductor quantum wells [1–3] and noble metals [3–6]), the in-plane effective mass is, at most, only weakly dependent on the sub-band index. The ability to deterministically engineer the effective mass or density of states of each sub-bands could have implications for technological applications which depend on quantum confinement, such as quantum cascade lasers [7], tunnel diodes [8], and photocatalysts [9].

Transition metal oxides offer inherent advantages for devices based on quantum confinement, owing to their unparalleled range of exotic electronic and magnetic properties, and to their high carrier densities and the tunability of their electronic structure [10]. Rutile IrO₂ is a technologically important transition metal oxide, exhibiting a large spin Hall effect for spin injection and detection [11], and is an efficient catalyst for the oxygen evolution reaction [12]. In these applications, the magnitude of the spin Hall angle and the catalytic activity depend sensitively on the effective mass, and therefore it is highly desirable to be able to tune the effective mass in a deterministic way.

Here, we demonstrate the ability to enhance the sub-band effective masses of atomically thin films of IrO₂

grown by oxide molecular-beam epitaxy (MBE) by up to a factor of six, as investigated by angle-resolved photoemission spectroscopy (ARPES). We show that the effective masses can be deliberately engineered by applying quantum confinement to a material with a highly non-parabolic, three-dimensional dispersion, thereby quantizing the values of k_z by selecting the number of monolayers in the material. This approach can be broadly applied to a wide class of other functional materials. In contrast to other mechanisms for tuning the effective mass, such as epitaxial strain [13] and crystallographic orientation [14] which produce changes on the order of tens of percents, the mechanism we report here originates specifically from quantum confinement and produces changes up to a factor of six. This behavior can be predicted based on a simple model of momentum discretization.

Fig. 1 presents an overview of the structural and transport properties of our ultrathin IrO₂ films, grown by MBE on (110)-oriented TiO₂ substrates. In addition to the sharp 110 and 220 Bragg reflections, we observe sharp and persistent finite thickness (Kiessig) fringes over nearly the entire range of measured angles, indicating atomically smooth surfaces and interfaces. X-ray rocking curves exhibit full width at half maxima (FWHM) on the order of 20–35 arc seconds, comparable to the substrate. Together with the step-and-terrace morphology revealed by atomic force microscopy (Fig. 1(b)) and the sharp (1 × 1) low energy electron diffraction pattern (Fig. 1(c)), these measurements establish the high structural quality of our ultrathin films. Further details of growth

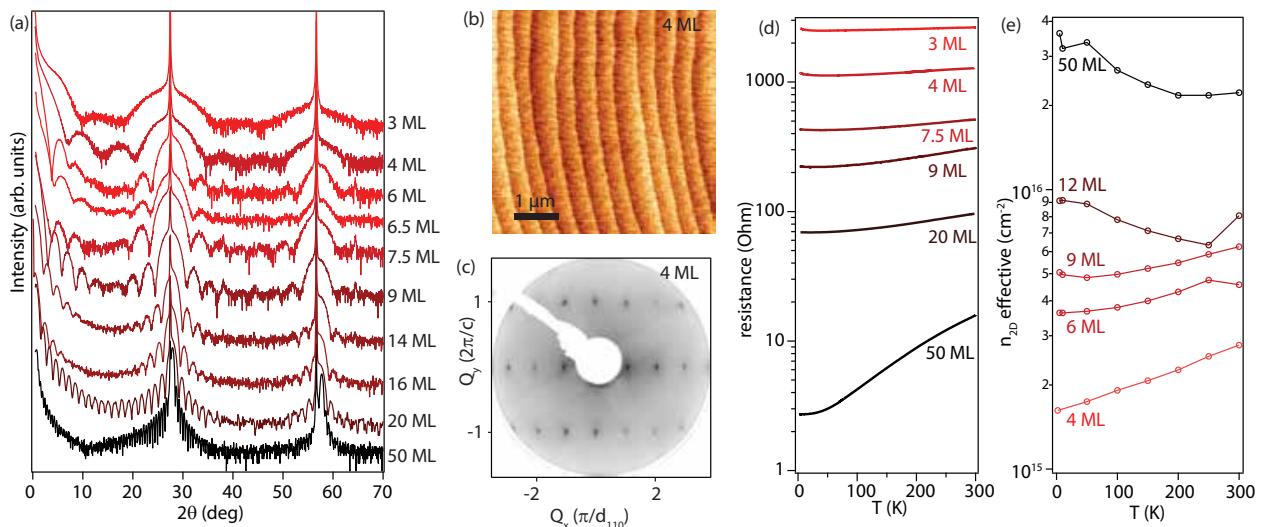


FIG. 1. Structural and transport characteristics of ultrathin IrO_2 thin films grown on (110) TiO_2 . (a) X-ray diffraction $\theta - 2\theta$ scans ($\text{Cu } K\alpha$). (b) Atomic force microscopy (AFM) topograph of a 4 ML thick film, with step heights corresponding to 1 ML. (c) Low energy electron diffraction (LEED, $h\nu = 150$ eV) pattern of the 4 ML film showing a sharp (1×1) pattern and indicating a well atomically ordered surface. (d) Resistance versus temperature measured along $[001]$, showing retained metallicity for all films. (e) Effective 2D carrier density (defined as inverse of the Hall coefficient, $1/R_H q$, where $q =$ fundamental charge) versus temperature, showing hole dominated transport.

and characterization are provided in the Supplemental and in Refs. [15] and [16].

Temperature dependent resistivity measurements reveal metallic behavior ($dR/dT > 0$) for all films down to 3 ML thickness (Fig. 1(d)). Below 40 K the 3 and 4 ML films show a slight upturn in resistance below 40 K. This metallicity in the atomically thin limit is already quite remarkable, in that the majority of ultrathin transition metal oxide thin films (e.g., $\text{La}_{1-x}\text{Sr}_x\text{MnO}_3$ [17], SrRuO_3 [18]) show thickness-driven metal-insulator transitions below approximately 4 unit cells. The 50 ML sample exhibits a residual resistivity of only $\rho_{4K} = 4 \mu\Omega\text{-cm}$, the lowest of any IrO_2 films reported to date [19–21], establishing the high quality of these samples. Hall effect measurements (Fig. 1(e)) indicated sheet carrier (hole-like) densities in the range of $10^{15} - 10^{16} \text{ cm}^{-2}$ ($n_{3D} \sim 10^{22} \text{ cm}^{-3}$). This number should, however, be treated only as approximate, due to the complex multiband nature of IrO_2 , which is also evidenced in the nontrivial temperature dependence. The effective three-dimensional carrier density sharply decreases for films with thickness less than 10 ML, indicating the strong effects of quantum confinement (Supplemental).

In Fig. 2(a) we show *in situ* ARPES measurements through the zone center $(0, 0)$ along $k_x \parallel [1\bar{1}0]$, measured using $\text{He } I\alpha$ ($h\nu = 21.2$ eV) photons. Along this cut, the bulk limit (50 ML) is characterized by highly dispersive hole-like (band max above E_F) and electron-like (≈ -1.5 eV band bottom) bands centered at $(0, 0)$ that are well described by density functional theory calculations that include spin-orbit coupling (Supplemental and Ref. [15]).

The bulk Fermi surface is highly three dimensional (Fig. 2(b)), and at this photon energy the ARPES measurement corresponds approximately to a slice at a constant perpendicular momentum of $k_z = (0.76 \pm 0.05)\pi/d_{110}$ [15].

As the film thickness is decreased, additional electron-like bands become readily apparent and evolve with film thickness. These additional states represent sub-bands generated by quantum confinement in the out-of-plane direction. In Fig. 2(a) the symbols represent the fitted sub-band dispersions as extracted from energy dispersion curve (EDC) fits near the band bottom and momentum distribution curve (MDC) fits near the Fermi energy. Measurement using a different photon energy, $h\nu = 40.8$ eV ($\text{He } II\alpha$), yields nearly identical dispersions, confirming the two-dimensional character of these sub-bands. The corresponding Fermi surface is nearly two-dimensional (Fig. 2(e)).

In Fig. 2(d) we plot the thickness evolution of the sub-band bottoms (circles), together with a fit (lines) to the Bohr-Sommerfeld quantization rule [4, 22], $2k_z(E)L + \phi(E) = 2\pi n$. Here $k_z(E)$ is the component of crystal momentum along the surface normal (from our GGA+SO calculation for bulk, Supplemental), $L = Nd_{110}$ is the total film thickness ($N =$ number of monolayers), $\phi(E)$ is the total phase shift resulting from the $\text{IrO}_2/\text{vacuum}$ and $\text{IrO}_2/\text{TiO}_2$ interfaces, and n is the quantum number. Excellent agreement with the data is obtained for an empirical fit to the phase of the form $\phi(E) = 4E$ (E in units of eV, ϕ in radians).

Closer examination of the sub-bands reveals that while

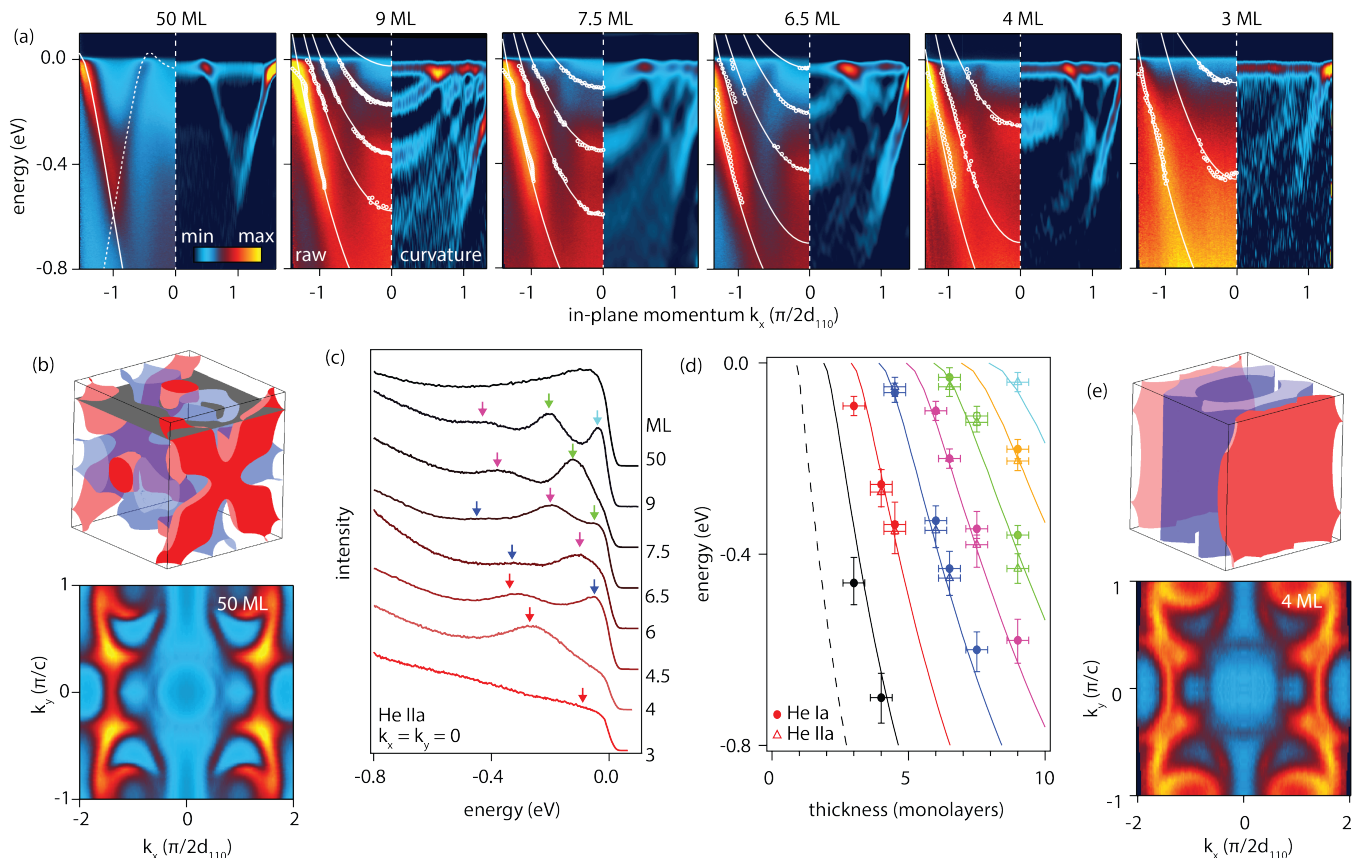


FIG. 2. ARPES measurements of metallic quantum well states. (a) Cuts along $k_x \parallel [1\bar{1}0]$ through $(0,0)$ for films 50 ML to 4 ML thick (measured using He I α). The left side of each plot in is the raw data and the right side is the second derivative ($-\frac{\partial^2 I}{\partial E^2}$, i.e., the curvature) of the raw data. Symbols denote EDC and MDC fits. Solid and dotted curves for 50 ML are the bulk GGA+SO calculation (including zone-folding at the (110) surface [15]), curves for 9 ML and thinner are empirical guides to the eye. (b) Three-dimensional GGA+SO Fermi surface (upper) and ARPES measured slice at constant k_z through Fermi surface (lower) in the bulk-like limit (50 ML). The constant $k_z = 0.76\pi/d_{110}$ slice is denoted by the gray plane through the three dimensional Fermi surface, as determined from fitting to a free-electron-like model of final states [15]. (c) Energy dispersion curves (EDCs, measured using He II α) through $(0,0)$ tracking the evolution of quantum well states. (d) Measured energy of the subband bottom versus film thickness (circles) and fit to the phase accumulation model (curves). Fits to the $n = 2$ subband for the 3 ML and 4 ML thick films (black data points) are extrapolated from EDC fits the the region near $k_{//} = 0$. (e) Schematic Fermi surface in the 2D limit (upper) and measured Fermi surface for the 4 thick ML film (lower).

the sub-bands furthest away from the Fermi energy (0 eV) are quite dispersive, those closer to the Fermi energy have much narrower bandwidths and hence have enhanced effective mass. To quantify the mass enhancement, we note that the sub-bands exhibit non-parabolic dispersions, and many are quite deep in binding energy, with band bottoms near 1 eV. Therefore the simple definition of effective mass as the second derivative of the energy with respect to momentum, commonly used for low density semiconductors, is not appropriate. To capture the mass relevant to near-Fermi level carriers, we employ the mass enhancement parameter

$$\tilde{M} = \frac{\partial E / \partial k}{\partial \epsilon^\alpha / \partial k} \Big|_{k=k_F^\alpha} = \frac{v_0}{v_F^\alpha}, \quad (1)$$

where v_0 is the bulk IrO₂ band velocity (from our

GGA+SO calculation) and v_F^α is the experimentally measured velocity of the sub-band α , both evaluated at the Fermi wavevector k_F^α of the sub-band as extracted from our EDC and MDC fits (Supplemental). This definition is identical to the one used in Refs. [23–25] for other quantum well systems, making it ideal for direct comparison with the literature. Figure 3 (filled symbols) presents the measured sub-band mass enhancement, exhibiting a remarkable six-fold mass enhancement of the near E_F bands, with respect to the bulk.

Our measurements for IrO₂ lie in striking contrast to nearly all other quantum well systems investigated to date, such as Ag/Cu(111) [5], Au/Ag(111) [4], GaAs/AlGaAs [1, 2], InAs (001) [3], and SrTiO₃ (001) [26, 27], for which the effective mass is weakly dependent (changes of order $\sim 10\%$) on sub-band index or

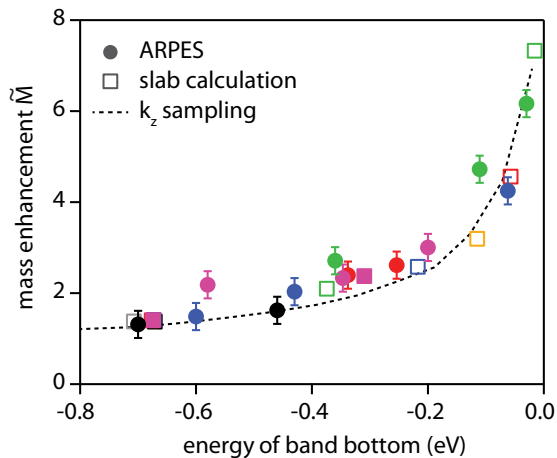


FIG. 3. Sub-band mass enhancement of IrO_2 extracted from ARPES (solid symbols), and comparison with DFT slab calculations (open symbols) and discrete k_z sampling of the bulk dispersion (dotted line). The color coding by sub-band index is the same as used in Fig. 2(d).

film thickness. The exceptions to this are low-density GaAs/AlGaAs heterostructures [28] and SrVO_3 ultrathin films [24], where in both cases, strong electron-electron interactions in the low-dimensional limit were invoked to explain the mass enhancements. For SrVO_3 , the reported mass enhancement was $\tilde{M} \approx 5$, using the same definition we use in Eqn 1 [23–25]. While electron correlations are indeed responsible for many emergent electronic and magnetic properties found in quantum materials, they also pose a barrier towards the deterministic design of devices and applications since the most common theoretical approaches such as density functional theory do not treat these correlations accurately. Indeed, the mass enhancements reported in GaAs/AlGaAs and SrVO_3 quantum wells cannot be explained using *ab initio* approaches, limiting their utility for engineering device applications.

As IrO_2 is also a transition metal oxide whose near- E_F states are comprised of partially filled d orbitals with strong spin-orbit coupling, it may be natural to assume that the large effective masses observed in the near- E_F sub-bands are also due to strong electron correlations, as in the case of ultrahigh mobility GaAs/AlGaAs [28] and the correlated metal SrVO_3 [24, 25]. Indeed, in IrO_2 , the iridium are coordinated in IrO_6 octahedra with a formally Ir^{4+} valence, just like in compounds such as Sr_2IrO_4 , where the combination of electron correlations from the Ir d orbitals and spin-orbit coupling give rise to a spin-orbit assisted Mott insulating state [29, 30], antiferromagnetism [31], broken symmetry states [32, 33], and the possibility of unconventional superconductivity [32–36]. On the other hand, recent ARPES studies of bulk IrO_2 demonstrated surprisingly good agreement between experiment and DFT calculations [15], suggesting that the electron correlations are relatively weak, in con-

trast to many other perovskite iridates.

To investigate whether these unusually large mass enhancements arise from electron correlations or other effects, we compare the experimental data to DFT slab calculations including spin-orbit coupling of thin IrO_2 films grown on (110) TiO_2 . In Fig. 4(a), we show a comparison between the slab calculation for an 8 ML thick film (left, black symbols) and the extracted ARPES dispersions (red circles) for the 7.5 ML thick IrO_2 film, which show remarkable agreement. This suggests that electron-electron interactions are not responsible for this large, sub-band-dependent mass enhancement, since the DFT calculations do not include any explicit local correlations ($U = 0$). In Fig. 3, we show a summary of \tilde{M} as a function band bottom energy for all the sub-bands measured in all of our thin films, together with a comparison from DFT slab calculations ranging between thicknesses of 2 to 10 ML, demonstrating good universal agreement. This implies that DFT-based approaches can be reliably employed to design IrO_2 -based quantum well systems with engineered, sub-band-dependent electronic properties. To our knowledge, this strong dependence of the sub-band effective mass with band filling is unprecedented, in the sense that this effect can be explained without the need for invoking either strong electron correlations [37] or interactions with the substrate [38–40].

We now show that the strong dependence of the sub-band effective mass arises when the band structure of bulk IrO_2 is quantized in the out-of-plane direction due to the finite film thickness. In contrast with simple metals such as Au (Ag) and low density semiconductors such as GaAs, the near-Fermi energy bulk electronic structure of IrO_2 is highly non-parabolic. When considering the effect of quantum confinement, for a film with a finite thickness of N atomic layers, k_z cannot be considered a continuous quantum number, but rather is discretized into N values (Fig. 4(b)). In a simple picture, each sub-band samples one of those discrete k_z values, in intervals of $\Delta k_z = \pi/(Nd)$, such that the in-plane electronic structure of each sub-band is approximately a k_x - k_y slice through the bulk electronic structure at a particular k_z value.

To illustrate the effect of k_z -sampling, in Fig. 4(a) we compare our ARPES measurement and DFT slab calculation for an $N = 8$ ML thick film, to a bulk calculation of IrO_2 where k_z is shown every $\pi/(Nd)$ interval (right side, blue curves). The in-plane mass enhancement extracted from k_z sampling of the bulk is plotted in Fig. 3 (dotted curve). The remarkable agreement between the ARPES data, the slab calculation, and the k_z -sampled calculation indicate that the strong sub-band dependence of the effective mass arises purely from quantum confinement of a non-parabolic band, without any appreciable substrate/film interactions or electron-electron correlations. In contrast, k_z -discretization of a parabolic band $E(\mathbf{k}) \sim \mathbf{kM}^{-1}\mathbf{k}^T$, where \mathbf{M} is the effective mass tensor and $\mathbf{k} = (k_x, k_y, k_z)$, recovers the simple behavior of

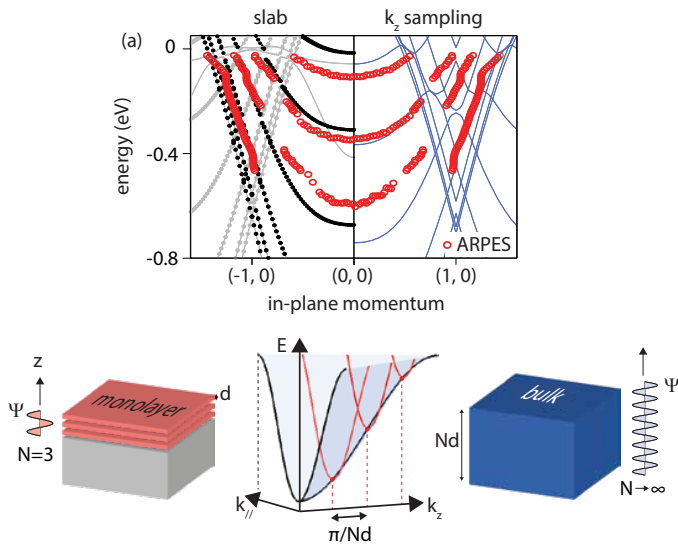


FIG. 4. Origin of mass enhancement. (a) ARPES dispersions for the 7.5 ML thick film (red circles) and comparison with a GGA+SO slab calculation for 8 ML thick IrO_2 (left, black symbols) and discrete k_z sampling of the GGA+SO bulk calculation (right, blue curves). (b) Schematic of how quantized subbands (E vs $k_{//}$) arise from discrete k_z sampling of the bulk dispersion $E(k_{//}, k_z)$. Sampling of k_z is in increments of $\pi/(Nd)$, where N is the number of monolayers and $d = d_{110}$ is the monolayer spacing.

effective mass being independent of sub-band (k_z) index.

In summary, using a combination of MBE and ARPES, we discovered that the effective mass of quantum well sub-bands in atomically thin IrO_2 films is energy dependent, with masses for the shallowest sub-bands enhanced as large as six times with respect to the bulk. This dramatic mass enhancement is far greater than observed in nearly any other material studied to date. By comparing the experimental data with density functional theory calculations of both finite slabs and bulk IrO_2 , we determine that the origin for this effect is the highly non-parabolic electronic structure of IrO_2 , which we speculate might arise from higher order hopping terms in the highly connected rutile structure. Quantum confinement in ultrathin films discretizes the out-of-plane band structure, giving rise to the observed phenomena reported here. This large mass enhancement can be accurately predicted from the bulk electronic structure, and does not depend on either complex substrate / film interactions or many-body electron-electron interactions, both of which can be very difficult to treat accurately. This suggests that careful consideration of the bulk electronic structure can be used to predict and engineer quantum well sub-bands with designer electronic properties. Potential applications include: tunnel diodes with precisely tuned transmission current profiles (which depend both on energy level spacings and the effective masses), photocatalysts with precisely tuned kinetics (via tunable adsor-

bate - metal d and s band overlap [9]), and increased spin Hall voltages for enhanced spin current detection (via increased electrical resistivity, without the introduction of impurities) [11].

See Supplemental Materials for details on sample growth and ARPES fitting, which includes Refs [41–43].

Acknowledgments. We thank Masaki Uchida and Yang Liu for helpful discussions. This work was supported by the National Science Foundation through the Platform for the Accelerated Realization, Analysis, and Discovery of Interface Materials (PARADIM; DMR-1539918), the Air Force Office of Scientific Research (Grants No. FA9550-12-1-0335 and FA2386-12-1-3103), and the Gordon and Betty Moore Foundation as part of the EPiQS initiative (GBMF3850). This research also utilized shared facilities supported by the Cornell Center for Materials Research through the MRSEC program (NSF DMR-1120296) and the Cornell Nanoscale Facility (Grant EECs-1542081), a member of the National Nanotechnology Coordinated Infrastructure. J.N.N. acknowledges support from the NSF Graduate Research Fellowship under grant no. DGE-1650441.

* Current address: Department of Materials Science and Engineering, University of Wisconsin, Madison WI 53706
 † kmshen@cornell.edu

- [1] A. T. Hatke, M. A. Zudov, J. D. Watson, M. J. Manfra, L. N. Pfeiffer, and K. W. West, *Phys. Rev. B* **87**, 161307 (2013), URL <https://link.aps.org/doi/10.1103/PhysRevB.87.161307>.
- [2] L. Smrčka, P. Vašek, J. Koláček, T. Jungwirth, and M. Cukr, *Phys. Rev. B* **51**, 18011 (1995), URL <https://link.aps.org/doi/10.1103/PhysRevB.51.18011>.
- [3] N. Olszowska, J. Lis, P. Ciochon, L. Walczak, E. G. Michel, and J. J. Kolodziej, *Phys. Rev. B* **94**, 115305 (2016), URL <https://link.aps.org/doi/10.1103/PhysRevB.94.115305>.
- [4] T.-C. Chiang, *Surface Science Reports* **39**, 181 (2000).
- [5] M. A. Mueller, T. Miller, and T.-C. Chiang, *Phys. Rev. B* **41**, 5214 (1990), URL <http://link.aps.org/doi/10.1103/PhysRevB.41.5214>.
- [6] J. Paggel, T. Miller, D.-A. Luh, and T.-C. Chiang, *Appl. Surf. Sci.* **162**, 78 (2000).
- [7] C. Gmachl, F. Capasso, D. L. Sivco, and A. Y. Cho, *Rep. Prog. Phys.* **64**, 1533 (2001).
- [8] M. Sweeny and J. Xu, *Appl. Phys. Lett.* **54**, 546 (1989).
- [9] B. Hammer and J. K. Nørskov, *Adv. Catal.* **45**, 71 (2000).
- [10] H. Hwang, Y. Iwasa, M. Kawasaki, B. Keimer, N. Nagaosa, and Y. Tokura, *Nat. Mater.* **11**, 103 (2012).
- [11] K. Fujiwara, Y. Fukuma, J. Matsuno, H. Idzuchi, Y. Nimi, Y. Otani, and H. Takagi, *Nat. Commun.* **4** (2013).
- [12] D.-Y. Kuo, J. K. Kawasaki, J. N. Nelson, J. Kloppenburg, G. Hautier, K. M. Shen, D. G. Schlom, and J. Suntivich, *J. Am. Chem. Soc.* **139**, 3473 (2017).
- [13] C. E. Dreyer, A. Janotti, and C. G. Van de Walle, *Applied Physics Letters* **102**, 142105 (2013).
- [14] S.-H. Park, *Journal of applied physics* **91**, 9904 (2002).

- [15] J. K. Kawasaki, M. Uchida, H. Paik, D. G. Schlom, and K. M. Shen, *Phys. Rev. B* **94**, 121104 (2016), URL <http://link.aps.org/doi/10.1103/PhysRevB.94.121104>.
- [16] J. K. Kawasaki, D. Baek, H. Paik, H. P. Nair, L. F. Kourkoutis, D. G. Schlom, and K. M. Shen, *Phys. Rev. Materials* **2**, 054206 (2018), URL <https://link.aps.org/doi/10.1103/PhysRevMaterials.2.054206>.
- [17] M. Izumi, Y. Ogimoto, Y. Okimoto, T. Manako, P. Ahmet, K. Nakajima, T. Chikyow, M. Kawasaki, and Y. Tokura, *Phys. Rev. B* **64**, 064429 (2001), URL <https://link.aps.org/doi/10.1103/PhysRevB.64.064429>.
- [18] D. Toyota, I. Ohkubo, H. Kumigashira, M. Oshima, T. Ohnishi, M. Lippmaa, M. Takizawa, A. Fujimori, K. Ono, M. Kawasaki, et al., *Appl. Phys. Lett.* **87**, 162508 (2005).
- [19] W. J. Kim, S. Y. Kim, C. H. Kim, C. H. Sohn, O. B. Korneta, S. C. Chae, and T. W. Noh, *Phys. Rev. B* **93**, 045104 (2016), URL <https://link.aps.org/doi/10.1103/PhysRevB.93.045104>.
- [20] X. Hou, R. Takahashi, T. Yamamoto, and M. Lippmaa, *Journal of Crystal Growth* **462**, 24 (2017).
- [21] M. El Khakani, M. Chaker, and E. Gat, *Applied physics letters* **69**, 2027 (1996).
- [22] T. Miller, A. Samsavar, G. Franklin, and T.-C. Chiang, *Phys. Rev. Lett.* **61**, 1404 (1988).
- [23] S. Okamoto, *Phys. Rev. B* **84**, 201305 (2011).
- [24] K. Yoshimatsu, K. Horiba, H. Kumigashira, T. Yoshida, A. Fujimori, and M. Oshima, *Science* **333**, 319 (2011).
- [25] M. Kobayashi, K. Yoshimatsu, E. Sakai, M. Kitamura, K. Horiba, A. Fujimori, and H. Kumigashira, *Phys. Rev. Lett.* **115**, 076801 (2015), URL <http://link.aps.org/doi/10.1103/PhysRevLett.115.076801>.
- [26] W. Meevasana, P. King, R. He, S. Mo, M. Hashimoto, A. Tamai, P. Songsiriritthigul, F. Baumberger, and Z. Shen, *Nat. Mater.* **10**, 114 (2011).
- [27] A. Santander-Syro, O. Copie, T. Kondo, F. Fortuna, S. Pailhes, R. Weht, X. Qiu, F. Bertran, A. Nicolaou, A. Taleb-Ibrahimi, et al., *Nature* **469**, 189 (2011).
- [28] Y.-W. Tan, J. Zhu, H. L. Stormer, L. N. Pfeiffer, K. W. Baldwin, and K. W. West, *Phys. Rev. Lett.* **94**, 016405 (2005), URL <http://link.aps.org/doi/10.1103/PhysRevLett.94.016405>.
- [29] B. Kim, H. Jin, S. Moon, J.-Y. Kim, B.-G. Park, C. Leem, J. Yu, T. Noh, C. Kim, S.-J. Oh, et al., *Phys. Rev. Lett.* **101**, 076402 (2008).
- [30] G. Jackeli and G. Khaliullin, *Phys. Rev. Lett.* **102**, 017205 (2009).
- [31] J. Matsuno, K. Ihara, S. Yamamura, H. Wadati, K. Ishii, V. V. Shankar, H.-Y. Kee, and H. Takagi, *Phys. Rev. Lett.* **114**, 247209 (2015).
- [32] Y. Kim, O. Krupin, J. Denlinger, A. Bostwick, E. Rotenberg, Q. Zhao, J. Mitchell, J. Allen, and B. Kim, *Science* **345**, 187 (2014).
- [33] Y. Kim, N. Sung, J. Denlinger, and B. Kim, *Nat. Phys.* **12**, 37 (2016).
- [34] H. Watanabe, T. Shirakawa, and S. Yunoki, *Phys. Rev. Lett.* **110**, 027002 (2013).
- [35] F. Wang and T. Senthil, *Phys. Rev. Lett.* **106**, 136402 (2011).
- [36] Y. Yan, M. Ren, H. Xu, B. Xie, R. Tao, H. Choi, N. Lee, Y. Choi, T. Zhang, and D. Feng, *Phys. Rev. X* **5**, 041018 (2015).
- [37] J. H. Dil, J. W. Kim, T. Kampen, K. Horn, and A. R. H. F. Erttema, *Phys. Rev. B* **73**, 161308 (2006), URL <https://link.aps.org/doi/10.1103/PhysRevB.73.161308>.
- [38] S.-J. Tang, C.-Y. Lee, C.-C. Huang, T.-R. Chang, C.-M. Cheng, K.-D. Tsuei, and H.-T. Jeng, *Appl. Phys. Lett.* **96**, 103106 (2010).
- [39] B. Slomski, F. Meier, J. Osterwalder, and J. H. Dil, *Phys. Rev. B* **83**, 035409 (2011).
- [40] Y. Liu, J. Paggel, M. Upton, T. Miller, and T.-C. Chiang, *Phys. Rev. B* **78**, 235437 (2008).
- [41] W. Ryden, A. Lawson, and C. Sartain, *Physics Letters A* **26**, 209 (1968).
- [42] A. Lanzara, P. Bogdanov, X. Zhou, S. Kellar, D. Feng, E. Lu, T. Yoshida, H. Eisaki, A. Fujimori, K. Kishio, et al., *Nature* **412**, 510 (2001).
- [43] Z. Zhong, Q. Zhang, and K. Held, *Phys. Rev. B* **88**, 125401 (2013), URL <https://link.aps.org/doi/10.1103/PhysRevB.88.125401>.